A R C H I V E O F M E C H A N I C A L E N G I N E E R I N G

VOL. LXIV 2017 Number 2

DOI: 10.1515/meceng-2017-0013

Key words: vertical-axis wind turbines, aerodynamics, computational fluid dynamics

KRZYSZTOF ROGOWSKI[1], *RYSZARD MAROŃSKI*[1], *JANUSZ PIECHNA*[1]

NUMERICAL ANALYSIS OF A SMALL-SIZE VERTICAL-AXIS WIND TURBINE PERFORMANCE AND AVERAGED FLOW PARAMETERS AROUND THE ROTOR

Small-scale vertical-axis wind turbines can be used as a source of electricity in rural and urban environments. According to the authors' knowledge, there are no validated simplified aerodynamic models of these wind turbines, therefore the use of more advanced techniques, such as for example the computational methods for fluid dynamics is justified. The paper contains performance analysis of the small-scale vertical-axis wind turbine with a large solidity. The averaged velocity field and the averaged static pressure distribution around the rotor have been also analyzed. All numerical results presented in this paper are obtained using the SST k-ω turbulence model. Computed power coefficients are in good agreement with the experimental results. A small change in the tip speed ratio significantly affects the velocity field. Obtained velocity fields can be further used as a base for simplified aerodynamic methods.

1. Introduction

Originally, the Darrieus wind turbine is a lift-driven vertical-axis wind turbine (VAWT) having a number of curved blades. The turbine patented in 1931 by G.J.M. Darrieus was designed for electricity generation. The blade curvature resembles the shape of a perfectly flexible cable. Due to the curvature, bending stresses of the blades are minimized during the rotation of the rotor. In the original version of the Darrieus wind turbine, each blade has a symmetric airfoil in its cross section. Blades are fixed to the rotating vertical tower. The lift-driven H-rotor, also called the Giromill or H-bar, is a modified version of the Darrieus wind turbine. This wind machine is equipped with straight blades attached to the tower with horizontal struts. In order to maximize the energy extracted from the wind, the blades of

[1] *Warsaw University of Technology, Institute of Aeronautics and Applied Mechanics, Warsaw, Poland. Emails: krogowski@meil.pw.edu.pl, maron@meil.pw.edu.pl, jpie@meil.pw.edu.pl*

the H-rotor are articulated [1–4]. Fig. 1 presents the small-size vertical axis wind turbine designed as a 3.5 kW wind machine and tested in the NRC 9 m × 9 m Low Speed Wind Tunnel in Ottawa [5].

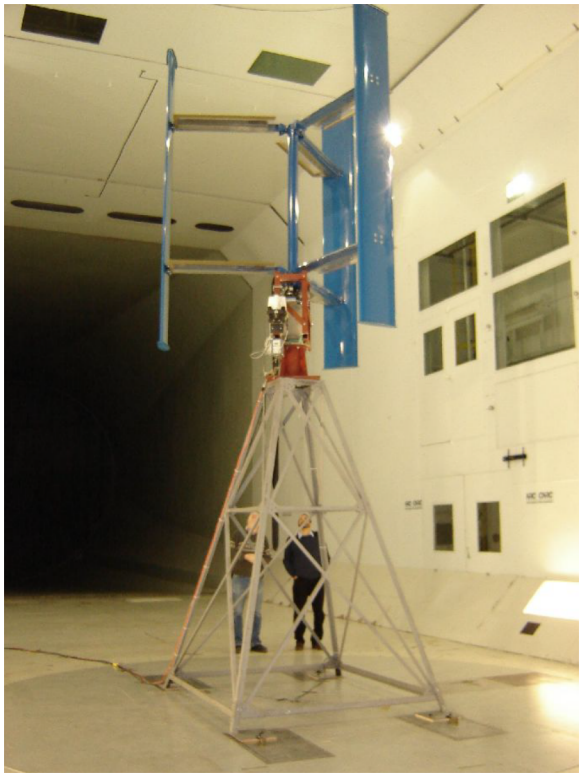

Fig. 1. Silhouette of the Darrieus-type turbine with a H-rotor [5]

Vertical axis wind turbines have become quite popular recently. Development of large-scale VAWTs is limited by saturation in the improvement of the aerodynamic performance of large-scale horizontal axis wind turbines (HAWTs). Islam et al. [6] predicted that, in the next two or three decades, VAWTs can dominate the technology of wind energy. Small-scale vertical axis wind turbines are designed for decentralized electricity generation in cities and rural areas [7]. The advantages of VAWTs are, for example: relatively high aerodynamic efficiency; the lack of the yaw system; lower manufacturing costs of the blades; simple tower construction and the possibility of placing a generator at the ground level [1]. Currently, the Darrieus concept is investigated for offshore applications [8, 9].

Over the years, many simplified aerodynamic models of vertical-axis wind turbines were developed. Islam et al. [10] classified these models into three categories: momentum models (streamtube models), vortex models and cascade models. One of the most common momentum-based model is the double multiple streamtube

model (DMS) developed by Paraschivoiu [3]. Because of the accuracy of the solution and the short time of calculation, this model is still successfully used in optimization of vertical axis wind-turbines [3, 11]. Momentum-based models are not efficient for an accurate estimation of the aerodynamic wake behind the rotor and for an accurate prediction of aerodynamic blade loads for large tip speed ratios, therefore Strickland et al. [12] developed the vortex model for the vertical-axis wind turbine applications. Ferreira et al. [13] simulated a two bladed VAWT using the following aerodynamic models: a multiple streamtube model, a double-multiple streamtube model, an actuator cylinder model, a 2D potential flow panel model, a 3D unsteady lifting line model, and a 2D conformal mapping unsteady vortex model. Finally, they concluded that streamtube models are inaccurate in comparison with the other four models.

There are many methods for determining aerodynamic derivatives [14]. Nowadays computational methods of fluid dynamics are increasingly used to simulate flow around the object. A single NACA 0015 airfoil in the Darrieus motion under dynamic stall conditions was investigated by Allet et al. [15]. The Reynolds-averaged Navier-Stokes equations were solved both with the algebraic Cebeci-Smith turbulence model and the nonequilibrium Johnson-King model. A 2D VAWT under dynamic stall conditions was investigated by Ferreira et al. [16]. The authors compared results of the unsteady aerodynamic blade loads for the following turbulence models: Spalart-Allmaras, k-ε, Large Eddy Simulation and Detached Eddy Simulation. Unsteady effects in the flow field around the 2D rotor were examined by Amet et al. [17] using the k-ω turbulence model. Large hysteresis loops of the lift and the drag coefficients were founded at low tip speed ratios.

New approaches for aerodynamic analysis of the Darrieus-type vertical axis wind turbines are based on the Navier-Stokes equations and the simplified aerodynamic models. Shen et al. [18] computed flow past a rotor with two NACA0012 blades using the 2D actuator surface technique. In this technique, the Navier-Stokes equations are used for the analysis of the flow around the two-dimensional rotor whereas two blades are represented by two actuator lines. Aerodynamic loads at each blade are computed using tabulated airfoil data.

The main purposes of this paper are:

a) Analysis of performance of the small-size Darrieus-type vertical-axis wind turbine with the large solidity.
b) Analysis of the averaged velocity field around the rotor of the wind turbine.
c) Analysis of the static pressure distribution near the rotor.

2. Aerodynamic loads and rotor performance

In order to explain the principle of operation of the wind turbine, the cross-section of the rotor rotating with the angular velocity ω is presented in Fig. 2. The velocity triangle consists of the tangential velocity of the blade V_T, the air velocity

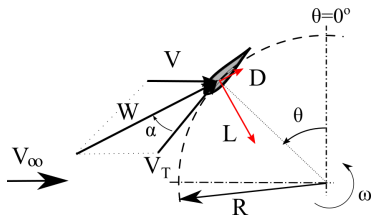

Fig. 2. Velocity vectors, angles and aerodynamic force components

in the rotor area V and the relative velocity W. The tangential velocity of the blade V_T depends on the rotor angular velocity ω and the rotor radius R:

$$V_T = \omega R. \tag{1}$$

The airfoil chord is tangent to the flight path of the point on the airfoil quarter chord line. The angle of attack is defined between the chord line and the relative velocity W. The relative velocity W and the angle of attack α vary with the azimuth position θ. The changing angle of attack is associated with the changing lift and drag forces L and D, respectively. Aerodynamic performance of the rotor and the kind of aerodynamic phenomena depends on the tip speed ratio (TSR) – the ratio of the tangential velocity of the blade and the wind velocity V_∞:

$$TSR = \frac{V_T}{V_\infty} = \frac{\omega R}{V_\infty}. \tag{2}$$

Assuming that $V = V_\infty$, at low tip speed ratios (e.g. TSR = 1) the angle of attack can achieve even $\pm 90^\circ$ and the effect of dynamic stall appears [19]. According to Laneville and Vittecoq [20], for high tip speed ratios, the rotor blade interacts with the aerodynamic wake from other rotor blades as well as from the blade itself. Aerodynamic forces, lift and drag, are perpendicular and parallel to the relative velocity W, respectively. These aerodynamic forces projected on a normal and a tangential to the blade trajectory produce normal and tangential blade loads, F_N and F_T, respectively. The aerodynamic blade loads are usually given as normal and tangential coefficient, c_N and c_T. According to geometric considerations (Fig. 2), the blade coefficients are as follows:

$$\begin{aligned} C_N &= C_L \cos\alpha + C_D \sin\alpha, \\ C_T &= C_L \sin\alpha - C_D \cos\alpha, \end{aligned} \tag{3}$$

where:

$$\begin{aligned} C_N &= \frac{F_N}{0.5\rho W^2 c}, \\ C_T &= \frac{F_T}{0.5\rho W^2 c}, \end{aligned} \tag{4}$$

where: c is airfoil chord and ρ is an air density.

The flow that passes a vertical-axis wind turbine is unsteady because aerodynamic forces depend on the azimuth θ. During the rotation of the rotor, fluctuations of the blade loads are significant. Therefore, the blade loads given by Eq. (3) are instantaneous and in order to compute the wind turbine performance the unsteady analysis has to be made. The performance of the wind turbine is called the power coefficient C_P which is the ratio of the turbine power extracted by the rotor blades P to the available power in an air stream of the same cross-sectional area as the rotor swept area A:

$$C_P = \frac{P}{0.5\rho A V_\infty^3}. \tag{5}$$

For the H-Darrieus wind turbine (Fig. 1), the rotor swept area is defined as $A = D\,H$, where D is the rotor diameter and H is the rotor height. The power produced by the turbine P can be given as:

$$P = T\omega, \tag{6}$$

where T is the average rotor torque produced by the rotor. The power coefficient given by the Eq. (5) depends on the tip speed ratio $C_P(TSR)$ in the following way:

$$C_P = TSR \cdot C_T = \frac{R\omega}{V_\infty} C_T, \tag{7}$$

where C_T is the average torque coefficient which is defined as:

$$C_T = \frac{T}{0.5\rho V_\infty^2 AR} \tag{8}$$

According to Paraschivoiu [3], typical vertical-axis wind turbines achieve maximum power coefficient $C_{P_{\max}} \approx 0.4$ at the tip speed ratio of around 6. However, the power coefficient depends also on the solidity σ and the number of blades N. The solidity is defined as [3]:

$$\sigma = \frac{Ncl}{A}, \tag{9}$$

where: l is the blade length (for H-Darius wind turbines $l = H$). Strickland et al. [12] and Claessens [21] used some different definition of the solidity for the H-Darrieus wind turbines:

$$\sigma = \frac{Nc}{R}. \tag{10}$$

For some wind turbines with high values of the solidity the maximum power coefficient can be observed for tip speed ratios much lower than 6 [5, 22].

3. Numerical model of the rotor

The two-dimensional model of vertical-axis wind turbine presented in this paper is developed based on the experimental wind turbine [5]. Silhouette of the experimental wind turbine is presented in Fig. 1. In this paper, the two-dimensional rotor geometry consisting of three blades is used for numerical analysis of the power coefficient, averaged velocity fields and averaged static pressure distributions. The rotating vertical shaft and struts are neglected in numerical investigations. The turbine height has been assumed to be infinite, therefore the rotor blades are represented by three symmetrical NACA 0015 airfoils with a chord of 0.4 m. The rotor diameter is assumed to be 2.5 m. The investigated wind turbine rotor is presented in Fig. 3. Operating parameters of the rotor such as the undisturbed flow velocity and angular velocities of the rotor are the same as during the experiment [5].

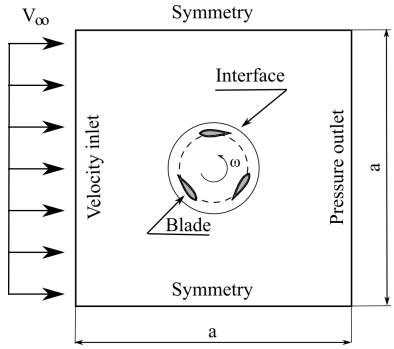

Fig. 3. Numerical model of the 2-D VAWT

The 2-D rotor has been simulated using the sliding mesh technique, therefore the mesh deformation is not considered in this work. The rotor is placed in the center of square virtual wind tunnel with the size of a. Based on the previous investigations of authors [23] and [24], the dimension a should be at least 10 times larger than the rotor diameter, therefore during this study the dimension a has been assumed 12 times larger than the rotor diameter. In order to use the sliding mesh model, a small circular area around the rotor is defined. This circular area can rotate with respect to the non-moving square area during numerical simulations. Between these two areas the interface zone is defined as presented in Fig. 3. The figure presents also all assumed boundary conditions.

During simulations, viscous flow has been considered and the shear stress transport (SST) k-ω turbulence model developed by Menter [25] has been employed for the analysis. Numerous publications confirm abilities of the two equation SST k-ω turbulence model in the VAWT applications [23, 26].

The domain presented in Fig. 3 is approximated by finite elements. The used hybrid mesh consists of structured mesh with quadrilateral elements near the blades and unstructured grid with triangle elements elsewhere. The mesh presented in

Fig. 4 is examined in the earlier works of the authors [23]. The entire grid consists of 192 540 finite elements. The thickness of the first layer of the structured mesh is $2 \cdot 10^{-6}$ m. For this value of the first layer thickness, the parameter $y+$ is obtained $\leqslant 1$. The structured part of the mesh consists of 15 layers with the growth rate of 1.2.

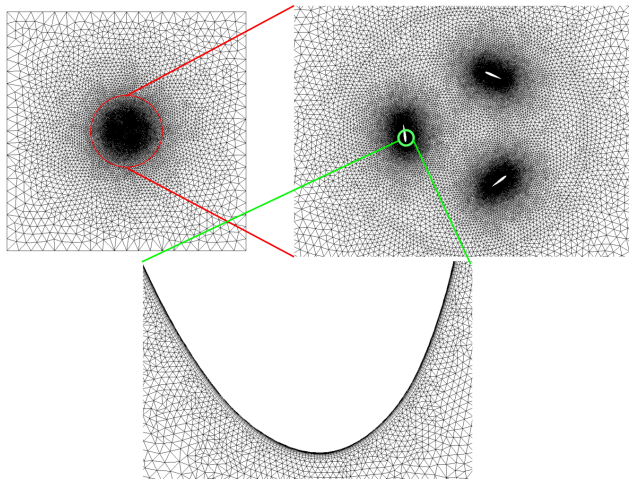

Fig. 4. Mesh

4. Averaged velocity field and static pressure distribution

A simple approach to aerodynamic analysis of Darrieus-type wind turbines is the one-dimensional (1-D) momentum theory. The theory fails for wind turbines with large solidity [21]. This is because in the Glauert momentum theory the air velocity components normal to the free stream velocity are neglected. Therefore, the purpose of this paper is to perform the analysis of averaged velocity field and averaged pressure distribution in the rotor area. The intention of the authors is to show the effect of a large solidity on the averaged flow field around a wind turbine rotor. The analysis has been performed using instantaneous flow parameters computed during unsteady analysis. The instantaneous flow parameters, such as velocities and static pressures, have been recorded at a time interval. The parameters have been investigated in a small square area around the rotor as presented in Fig. 5. A grid of checkpoints is specified in the square area. The resolution of the grid has been established: $\Delta x/\Delta y = 0.05\,\mathrm{m}/0.025\,\mathrm{m}$. Using these checkpoints, the static pressure and two air velocity components: parallel and perpendicular to the free stream velocity, u and v, respectively, have been recorded at the specified time interval. The time interval corresponds to the rotation of the rotor by one degree. The results of velocities and pressures are averaged over time corresponding to one complete revolution of the rotor.

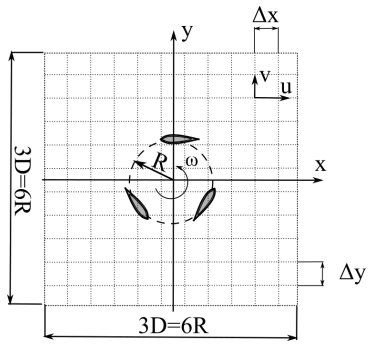

Fig. 5. Square grid of checkpoints around the rotor for recording pressure and velocity data

5. Results and discussion

This article presents the results of the rotor power coefficients as functions of the tip speed ratio. Moreover, the results of averaged velocity fields and averaged static pressure distributions near the wind turbine rotor are also investigated. Velocities are shown using vectors and profiles.

5.1. Power coefficient

The power coefficient is given as a function of a tip speed ratio Eq. (7). The comparison between numerical and experimental results of the power coefficient is qualitative rather than quantitative, because in the numerical model aerodynamic effects of the blade tip, struts and the rotating shaft are not considered. There are some investigations showing that the finite aspect ratio of the H-rotors slightly affects the power coefficient [3, 27]. The maximum power coefficient of the experimental wind turbine is 0.28 at the tip speed ratio of 1.5 – Fig. 6. Numerical analysis has shown that the maximum power coefficient is expected at a higher tip speed ratio. Since the wind turbine performance has been simulated up to the

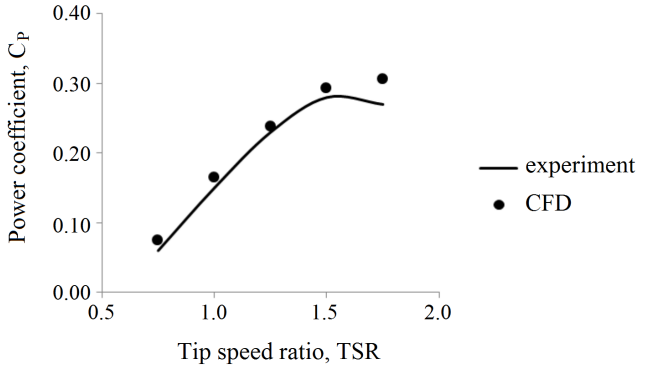

Fig. 6. Power coefficient vs. tip speed ratio

tip speed ratio of 1.75, the numerical maximum power coefficient is unknown. As expected, for the tip speed ratios of 1.5 and 1.75 the computed power coefficients are higher in comparison with the experiment. Resemblance between experimental and numerical power coefficients at low tip speed ratios seems to be too optimistic. Usually, CFD methods overestimate the results of the rotor power in this range of tip speed ratios because of large angles of attack and dynamic stall effects.

5.2. Velocity field in the rotor area

Velocity fields around the vertical-axis wind turbine are presented by using velocity vectors at two tip speed ratios: 1.25 and 1.75 (Fig. 7). In both cases, the undisturbed flow velocity is the same, whereas an angular velocity of the rotor is 10 rad/sec for the rotor operating at TSR of 1.25 and 14 rad/sec at TSR of 1.75. It

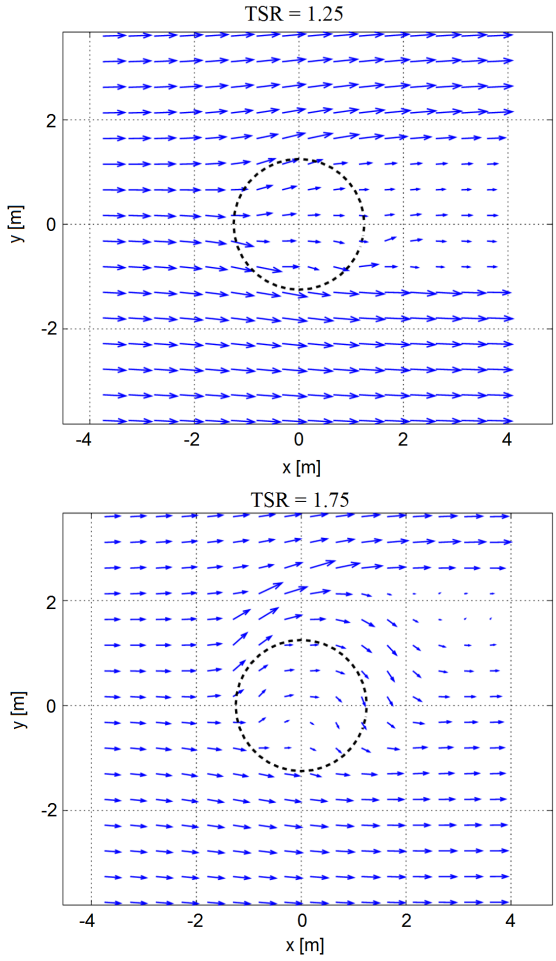

Fig. 7. Velocity vectors around the rotor for two tip speed ratios

is clearly seen from Fig. 7 that velocity fields differ significantly from each other. At TSR of 1.25, the deviation of the flow is very slight. This means that averaged values of v-components are very low. For the TSR of 1.75, large deviation of the flow is observed at the azimuth range between −90 deg. and 90 deg. (according to the azimuth position definition presented in Fig. 2). Fig. 8 shows the u-velocity profiles for two values of tip speed ratio 1.25 and 1.75 at the distance of one rotor diameter downstream from the rotor (or at the distance of $3R$ downstream from the rotor axis of rotation). As it can be seen from this figure, for the TSR of 1.25 the velocity profile is even symmetrical while for the TSR of 1.75 the asymmetric velocity profile is visible.

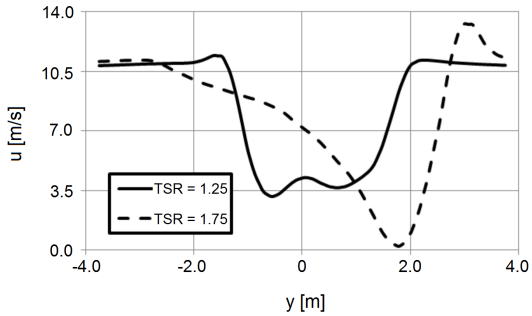

Fig. 8. Profiles of averaged u-velocities at the distance $3R$ downstream from the rotor axis of rotation

5.3. Static pressure distribution

In this article, the static pressure is referenced to the operating pressure which is the static pressure of undisturbed flow. The operating pressure is equal to 101 325 Pa. Fig. 9 presents profiles of the static pressure in front of and behind the rotor, that is for the coordinates $x = -3.75$ m and $x = 3.75$ m (Fig. 5). For comparison, the results are given for the tip speed ratio of 1.25 and 1.75. As it can be seen from

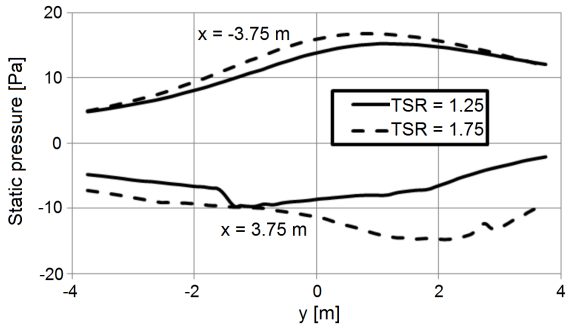

Fig. 9. Static pressure distributions at $x = -3.75$ m and $x = 3.75$ m

this figure, in both cases the results of the static pressure are similar to each other for $x = -3.75$ m and they are different for $x = 3.75$ m. The larger static pressure drop is observed for the higher tip speed ratio.

The averaged static pressure around the rotor has been also investigated. The static pressure has been computed near trajectories of the rotor blades at two circles with radii of $R + 0.5c$ and $R - 0.5c$, where R is the rotor radius and c is the chord length. The results of the static pressure as a function of the azimuth for two tip speed ratios separately are presented in Fig. 10. Moreover, the comparison between

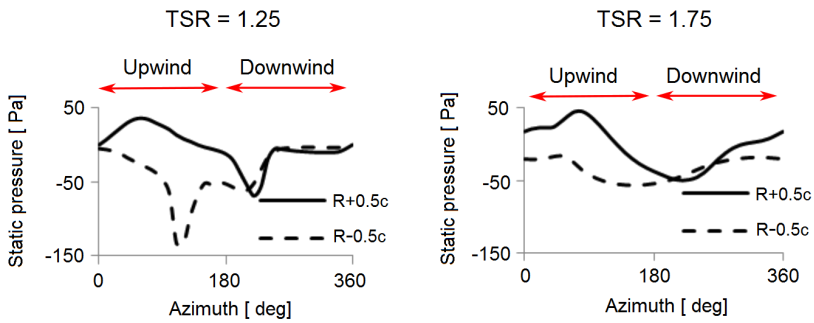

Fig. 10. Static pressure distribution around the rotor trajectory vs. azimuth position

the static pressure distribution on the circle with the radius of $R + 0.5c$ for two tip speed ratios is shown in Fig. 11. As it can be seen from Fig. 10, differences in air pressure are visible mainly at the upwind part of the rotor, i.e., for the azimuth in the range between 0 deg. and 180 deg. For the downwind part of the rotor, differences in air pressure are very low, especially for the rotor operating at the tip speed ratio of 1.25. It can be noticed form Figs. 10 and 11 that for the tip speed ratio of 1.25 the static pressure is almost constant at the azimuth range between 260 deg. and 360 deg.

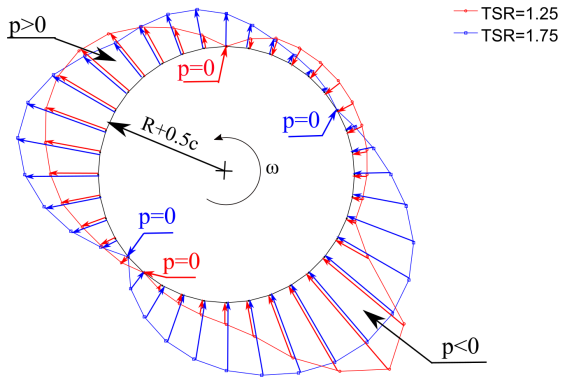

Fig. 11. Static pressure distribution around the rotor for two tip speed ratios

6. Conclusions

The purposes of the paper were the analyses of the wind turbine performance and the averaged flow parameters. Performed numerical analyses showed that:

1. The results of the power coefficient obtained using the SST k-ω turbulence model seem to be satisfactory at the whole tip speed ratio range.
2. For lover tip speed ratios, the results of the power coefficient very well correspond to the experimental measurement. This may indicate less impact of dynamic stall effects. Moreover, tree-dimensional aerodynamic effects of struts, tower etc. can be neglected for this range of the tip speed ratio. Therefore, these effects have to be more investigated in the future.
3. Averaged velocity field significantly depends on the tip speed ratio. For the rotor operating at lower tip speed ratios, velocity profile becomes more asymmetric in relation to higher tip speed ratios.
4. Contrary to the 1-D momentum theory, CFD methods show that the velocities normal to the free stream velocity cannot be neglected.
5. As the tip speed ratio increases, the static pressure difference increases in the area before and after the Darrieus-type rotor.
6. For the downwind part of the rotor, the differences in the static pressure at the blade trajectory are neglected, especially for the lower tip speed ratio. This means that the blade of VAWT with a large solidity does not work at this part of the rotor.
7. Future authors' investigations should be focused on employing obtained velocity fields for developing simplified aerodynamic methods for performance analysis of small-scale vertical-axis wind turbines with large solidity.

Manuscript received by Editorial Board, September 14, 2016;
final version, March 26, 2017.

References

[1] B.F. Blackwell. The vertical-axis wind turbine "How it works". Energy Report, SLA-74-0160, Sandia Laboratories, 1974.

[2] K. Jankowski. *Vertical axis turbine of Darrieus h-type with variable blade incidence angle concept design*. M.Sc. Thesis, Warsaw University of Technology, Poland, 2009.

[3] I. Paraschivoiu. *Wind Turbine Design: With Emphasis on Darrieus Concept*. Polytechnic International Press, Canada, 2002.

[4] I. Paraschivoiu, O. Trifu, and Saeed F. H-Darrieus wind turbine with blade pitch control. *International Journal of Rotating Machinery*, 2009:ID 505343, 2009. doi: 10.1155/2009/505343.

[5] R. Bravo, S. Tullis, and S. Ziada. Performance testing of a small vertical-axis wind turbine. In *Proceedings of the 21st Canadian Congress of Applied Mechanics CANCAM*, Toronto, Canada, 7-9 June 2007.

[6] M.R. Islam, S. Mekhilef, and R. Saidur. Progress and recent trends of wind energy technology. *Renewable and Sustainable Energy Reviews*, 21:456–468, 2013. doi: 10.1016/j.rser.2013.01.007.

[7] F. Scheurich, T.M. Fletcher, and R.E. Brown. The influence of blade curvature and helical blade twist on the performance of a vertical-axis wind turbine. In *48th AIAA Aerospace Sciences Meeting Including the New Horizons Forum and Aerospace Exposition*, Orlando, USA, 4-7 Jan. 2010. doi: 10.2514/6.2010-1579.

[8] H.A. Madsen, T.J. Larsen, U.S. Paulsen, and L. Vita. Implementation of the actuator cylinder flow model in the HAWC2 code for aeroelastic simulations on vertical axis wind turbines. In *Proceedings of 51st AIAA Aerospace Sciences Meeting including the New Horizons Forum and Aerospace Exposition*, Dallas, USA, 7-10 Jan. 2013. doi:10.2514/6.2013-913.

[9] W. Tjiu, T. Marnoto, S. Mat, M.H. Ruslan, and K. Sopian. Darrieus vertical axis wind turbine for power generation II: Challenges in HAWT and the opportunity of multi-megawatt Darrieus VAWT development. *Renewable Energy*, 75:560–571, March 2015. 10.1016/j.renene.2014.10.039.

[10] M. Islam, D.S.K. Ting, and A. Fartaj. Aerodynamic models for Darrieus-type straight-bladed vertical axis wind turbines. *Renewable and Sustainable Energy Reviews*, 12(4):1087–1109, 2008. doi: 10.1016/j.rser.2006.10.023.

[11] M Abdul Akbar and V Mustafa. A new approach for optimization of vertical axis wind turbines. *Journal of Wind Engineering and Industrial Aerodynamics*, 153:34–45, 2016. doi: 10.1016/j.jweia.2016.03.006.

[12] J.H. Strickland, T. Smith, and K. Sun. A vortex model of the Darrieus turbine: An analytical and experimental study. Report SAND81-7017, Sandia National Laboratories, 1981.

[13] C.S. Ferreira, H.A. Madsen, M. Barone, B. Roscher, P. Deglaire, and I. Arduin. Comparison of aerodynamic models for vertical axis wind turbines. *Journal of Physics: Conference Series*, 524(1):012125, 2014. doi: 10.1088/1742-6596/524/1/012125.

[14] P. Lichota and D.A. Noreña. A priori model inclusion in the multisine maneuver design. In *17th International Carpathian Control Conference (ICCC)*, pages 440–445, Tatranska Lomnica, Slovakia, 29 May – 1 June 2016. doi: 10.1109/CarpathianCC.2016.7501138.

[15] A. Allet, S. Hallé, and I. Paraschivoiu. Numerical simulation of dynamic stall around an airfoil in Darrieus motion. *Journal of Solar Energy Engineering*, 121:69–76, 1999. 10.1115/1.2888145.

[16] C.S. Ferreira, H. Bijl, G. van Bussel, and G. van Kuik. Simulating dynamic stall in a 2D VAWT: modeling strategy, verification and validation with particle image velocimetry data. *Journal of Physics: Conference Series*, 75:012023, 2007. doi: 10.1088/1742-6596/75/1/012023.

[17] E. Amet, T. Maître, C. Pellone, and J.L. Achard. 2D numerical simulations of blade-vortex interaction in a Darrieus turbine. *Journal of Fluids Engineering*, 131(11):111103, 2009. doi: 10.1115/1.4000258.

[18] W.Z. Shen, J.H. Zhang, and J.N. Sørensen. The actuator surface model: a new Navier-Stokes based model for rotor computations. *Journal of Solar Energy Engineering*, 131(1):011002, 2009. doi: 10.1115/1.3027502.

[19] F. Schuerich and R.E. Brown. Effect of dynamic stall on the aerodynamics of vertical-axis wind turbines. *AIAA journal*, 49(11):2511–2521, 2011. doi: 10.2514/1.J051060.

[20] A. Laneville and P. Vittecoq. Dynamic stall: the case of the vertical axis wind turbine. *Journal of Solar Energy Engineering*, 108(2):140–145, 1986. doi: 10.1115/1.3268081.

[21] M.C. Claessens. *The Design and Testing of Airfoils for Application in Small Vertical Axis Wind Turbines*. M.Sc. Thesis, Delft University of Technology, The Netherlands, 2006.

[22] P. Marsh, D. Ranmuthugala, I. Penesis, and G. Thomas. Three dimensional numerical simulations of a straight-bladed vertical axis tidal turbine. In *18th Australasian Fluid Mechanics Conference*, Launceston, Australia, 3-7 December 2012.

[23] K. Rogowski. *Analysis of Performance of the Darrieus Wind Turbines*. Ph.D. Thesis, Warsaw University of Technology, Poland, 2014.

[24] K. Rogowski and R. Maroński. CFD computation of the Savonius rotor. *Journal of Theoretical and Applied Mechanics*, 53(1):37–45, 2015. doi: 10.15632/jtam-pl.53.1.37.

[25] F.R. Menter. Two-equation eddy-viscosity turbulence models for engineering applications. *AIAA Journal*, 32(8):1598–1605, 1994. doi: 10.2514/3.12149.

[26] O. Guerri, A. Sakout, and K. Bouhadef. Simulations of the fluid flow around a rotating vertical axis wind turbine. *Wind Engineering*, 31(3):149–163, 2007. doi: 10.1260/030952407781998819.

[27] F. Scheurich, T.M. Fletcher, and R.E. Brown. Simulating the aerodynamic performance and wake dynamics of a vertical-axis wind turbine. *Wind Energy*, 14(2):159–177, 2011. doi: 10.1002/we.409.